PHYSICAL REVIEW A VOLUME 23, NUMBER 1 JANUARY 1981

Energy-transfer processes in decaying helium-copper gaseous plasmas

D. W. Ernie and H. J. Oskam
Department of Electrical Engineering, University of Minnesota, Minneapolis, Minnesota 55455
(Received 14 July 1980)

The time dependences of 35 Cu II energy levels between 15.96 and 24.62 eV were studied using light emission and absorption spectroscopy during the afterglow of a sputtered He-Cu hollow cathode discharge. By measuring the decay of the $He^m(2^3S)$ and $Cu(4s^2S_{1/2})$ densities, it was possible to determine the helium species [He^+, He_2^+, $He^m(2^3S)$, and $He_2^m(a^3\Sigma_u^+)$] responsible for production of the Cu II states. The Cu II levels between 22.7 and 24.62 eV are produced, either directly or by cascading, by charge exchange between He^+ and Cu. The Cu II levels between 15.96 and 21.41 eV are produced by charge exchange between He_2^+ and Cu. No evidence was found for the production of Cu II states by the Penning ionization of Cu by $He^m(2^3S)$ or $He_2^m(a^3\Sigma_u^+)$. A value of 430 ± 10 $cm^2\,sec^{-1}$ Torr was measured for the diffusion coefficient of $Cu(4s^2S_{1/2})$ in helium. The time dependence of the sputtered $Cu(4s^2S_{1/2})$ radial density profile was also investigated theoretically during the discharge sequence.

I. INTRODUCTION

During the past decade, laser action has been detected in discharges produced in several helium-metal vapor systems including He-Cd, He-Zn, He-Se, He-Cu, He-Ag, He-Au, and others.[1-7] These systems utilize population inversions achieved between excited states of the singly ionized metal ions by energy transfer from the various active helium species. Studies of decaying gaseous plasmas (afterglows) conducted on gas discharges in the He-Cd, He-Zn, and He-Se systems have indicated that the predominant energy-transfer mechanisms are the thermal-energy charge-transfer reaction

$$He^+ + M \rightarrow (M^+)^* + He + \Delta E \qquad (1)$$

and the Penning-ionization reaction

$$He^m(2^3S) + M \rightarrow (M^+)^* + He + e + \Delta E\,, \qquad (2)$$

where M is the ground state of the metal atom, $(M^+)^*$ is an excited state of the singly ionized metal ion, and ΔE is the energy defect.[8,9] Investigations of reaction (1) have shown that the charge-transfer cross section is largest for $0 < \Delta E < 0.6$ eV.[8,10,11] For reaction (2) there are indications that the Penning-ionization cross sections increase with increasing energy defect, being the largest for production of the metal-ion ground state.[10]

While reactions (1) and (2) have been extensively studied for systems involving higher vapor pressure metals such as Cd, Zn, Se, and Cs, energy-transfer reactions for systems involving lower vapor pressure metals such as Cu, Ag, and Au have not been directly determined. In the former systems, sufficient metal-atom vapor densities ($>10^{11}$ atoms/cm^3) can be achieved by auxiliary heating of the discharge region to temperatures of 150–370 °C. Standard afterglow techniques can then be employed to determine the energy-transfer mechanisms.[9,12] In the case of lower vapor pressure metals, however, temperatures of over 700 °C are required to obtain similar metal-atom densities. Sputtering in a hollow cathode discharge configuration has thus been employed to achieve the required metal-atom density in such laser systems.[4-7] Afterglow studies employing this discharge configuration are complicated, however, since the initial sputtered metal-atom density achieved is a function of discharge current, pulse width, and helium pressure. In addition, the decay of the metal-atom density during the afterglow due to diffusion of the metal atoms to the cathode wall must be included in the analysis of the experimental data.

The He-Cu system is a good candidate for investigating energy-transfer mechanisms between active helium species and low vapor pressure metals. The sputtering rate for Cu by helium is the largest of any metal,[13] providing higher sputtered metal-atom densities for a given discharge current. In addition, as can be seen in Fig. 1, the energy coincidence between the active helium species and various Cu II energy levels can lead to the charge-transfer reactions

$$He^+ + Cu \rightarrow (Cu^+)^* + He \qquad (3)$$

and

$$He_2^+ + Cu \rightarrow (Cu^+)^* + 2He\,, \qquad (4)$$

and to the Penning-ionization reactions

$$He^m(2^3S) + Cu \rightarrow (Cu^+)^* + He + e \qquad (5)$$

and

$$He_2^m(a^3\Sigma_u^+) + Cu \rightarrow (Cu^+)^* + 2He + e\,, \qquad (6)$$

where Cu is the ground-state copper atom

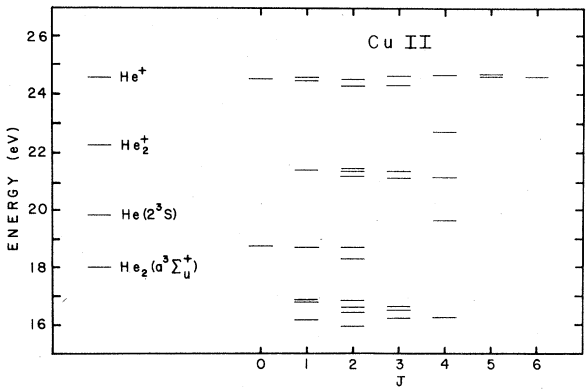

FIG. 1. Energy level diagram for monitored Cu II energy states, He^+, He_2^+, $He^m(2^3S)$, and $He_2^m(a^3\Sigma_u^+)$. Only the lowest vibrational level ($\nu=0$) is included for He_2^+ and $He_2^m(a^3\Sigma_u^+)$.

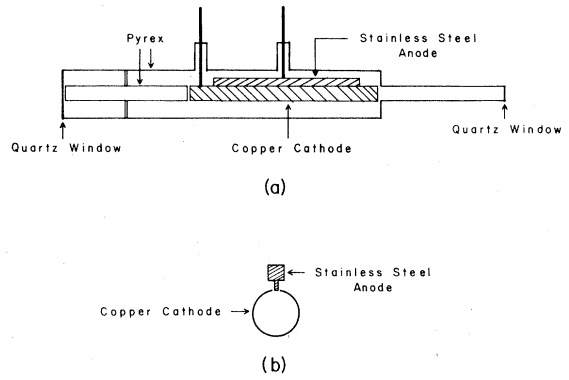

FIG. 2. Schematic diagram of the discharge-tube configuration.

$Cu(4s^2\,S_{1/2})$. Laser action has been reported utilizing several Cu II spectral lines in a He-Cu discharge and it was proposed that (3) and (5) are the predominant energy-transfer reactions.[5]

This paper presents measurements relating to processes (3)–(6) in the stationary afterglow of a He-Cu hollow cathode discharge. Cathode sputtering was used to create $Cu(4s^2\,S_{1/2})$ densities greater than 10^{10} atoms/cm^3 at the beginning of the afterglow period in 2 to 16 Torr of helium. The time dependence of the sputtered radial $Cu(4s^2\,S_{1/2})$ density profile during the discharge sequence was modeled to determine the time scale required to achieve a copper density profile in the active discharge which would decay close to the fundamental diffusion mode within a few hundred microseconds into the afterglow. Light emission and absorption spectroscopy were used to study the afterglow decay rates of the helium excited species, the singly ionized copper excited states, and the $Cu(4s^2\,S_{1/2})$ atoms. From the data, it was possible to determine the specific energy-transfer processes responsible for the production of Cu II energy levels. The diffusion coefficient of $Cu(4s^2\,S_{1/2})$ in helium was also obtained.

II. EXPERIMENTAL METHOD

The gas handling system used in the experiment was of the standard ultrahigh vacuum type and achieved a background pressure of 10^{-9} Torr after bakeout at 350 °C for 24 h. Research grade helium gas in one liter pyrex flasks was used. The helium was further purified by the cataphoretic segregation process in order to remove impurities such as neon. Final impurity levels in the helium gas were estimated to be less than one part per ten million.

Figure 2(a) is a schematic drawing of the discharge-tube configuration. The entire electrode assembly was enclosed in a pyrex tube with quartz end windows. The main discharge region consisted of a cylindrical copper cathode 15 cm long and 1.1 cm in diameter made of oxygen-free high-conductivity (OFHC) copper. This tube contained a 2-mm axial slit into which was inserted the knife edge of a stainless steel anode, as shown in the cross sectional view in Fig. 2(b). Pyrex tubing of the same inside diameter as the copper cathode was used at both ends of the copper tube and separated from it by 1–2 mm. This configuration maintained the cylindrical geometry of the discharge region, while preventing excessive covering of the quartz end windows and electrode feedthroughs by copper vapor.

The discharge configuration had a characteristic diffusion length $\Lambda = 0.23$ cm. The main discharge was produced by a pulsed dc voltage of 400–600 V with pulse widths of 0.4–0.8 msec and currents of 20 mA to 6 A. An auxiliary wire electrode was placed outside one end of the slit in the copper cathode and a 0.4-mA dc discharge was maintained between it and the cathode. This was required to achieve reliable breakdown during the main discharge pulse. The cathode temperature at high currents was maintained below 100 °C by controlling the duty cycle of the discharge pulse.

A capillary discharge light-source tube containing 2.5 Torr of helium was used for the absorption measurements on $He^m(2^3S)$. The light-source tube for the absorption studies on $Cu(4s^2\,S_{1/2})$ consisted of a cylindrical OFHC copper hollow cathode, a wire anode along the axis of the cathode, and a flat quartz end window spaced several centimeters from the cathode. The copper light source contained 5 Torr of helium and utilized sputtering to produce the necessary copper vapor

density. The emission from the two light-source tubes was collimated and passed axially down the absorption tube. The 388.9-nm helium line was used for the absorption studies on the $He^m(2^3S)$ species. The 324.8- and 327.4-nm Cu I resonance lines were used to monitor the $Cu(4S^2\,S_{1/2})$ density. These spectral lines and those observed in emission from Cu I, Cu II, and He I were analyzed using a Jarrell-Ash 0.5-m Ebert monochromator, and detected by a thermoelectrically cooled EMI (S-20) photomultiplier.

The photomultiplier was operated in the pulse-counting mode. The pulses were counted and stored in a minicomputer-controlled multichannel-scaling system. In the absorption studies, the background signal due to light emission from within the absorption tube was subtracted from the total transmitted signal. The requirement that the absorber density be low in order to have a direct proportionality between absorber number density and fractional absorption restricts measurements to fractional absorptions less than 10%.[14] The minimum detectable absorption was on the order of 0.1%, owing to statistical fluctuations in the signal level.

III. COPPER DENSITY PROFILE

In this experiment, the $Cu(4s^2\,S_{1/2})$ density is produced by sputtering and thus is a function of the spatial coordinates and time. It was necessary to accurately model this function during the discharge sequence. This was done in order to determine the time scale in the active discharge required to achieve a Cu density profile which would decay close to the fundamental diffusion mode within a few hundred microseconds into the afterglow. This is important since the data analysis of the afterglow is simplified when the relevant species' densities all have the fundamental mode spatial distribution.

During the active discharge, the Cu density builds up as copper atoms are sputtered into the discharge region by ions which have crossed the cathode fall region and strike the cathode surface at high energies. Studies indicate the sputtered copper atoms leave the cathode surface with energies on the order of 1 eV.[15] They are thermalized within 0.5 mm of the cathode surface,[16] and proceed by diffusion into the discharge region. In the afterglow, the ions have insufficient energy to cause sputtering and the Cu density decays as copper diffuses to the walls. The afterglow Cu density can also be perturbed by the destruction of Cu atoms by reactions (3)–(6). However, this effect is minimal under our experimental conditions.[17]

If it is assumed that the discharge region is cylindrical and of infinite length, the Cu density has only a radial spatial dependence and is determined by the diffusion equation

$$\frac{\partial n(r,t)}{\partial t} = D\left(\frac{\partial^2 n(r,t)}{\partial r^2} + \frac{1}{r}\frac{\partial n(r,t)}{\partial r}\right), \tag{7}$$

where $n(r,t)$ is the $Cu(4s^2\,S_{1/2})$ density, r is the radial distance from the axis of the discharge region, and D is the diffusion coefficient of copper atoms in helium. In order to derive the boundary conditions at the cathode surface $r=a$, it can be noted that the radially inward Cu flux $\Gamma_-(r,t)$ is given by[18]

$$\Gamma_-(r,t) = \tfrac{1}{4}n(r,t)\bar{v} - \tfrac{1}{2}\vec{\Gamma}(r,t)\cdot\hat{r}\,,$$

where $\bar{v}$ is the average Cu thermal velocity and $\vec{\Gamma}(r,t)$ is the net Cu flux. The net flux is given by

$$\vec{\Gamma}(r,t) = -D\,\frac{\partial n(r,t)}{\partial r}\,\hat{r}\,.$$

In addition, if it is assumed that all Cu atoms striking the cathode surface remain there, $\Gamma_-(a,t)$ is the sputtering rate Γ_s of Cu at the cathode surface ($\Gamma_s = 0$ during the afterglow). Therefore, the boundary condition is

$$\left.\frac{\partial n(r,t)}{\partial r}\right|_{r=a} = \frac{4\Gamma_s - n(a,t)\,\bar{v}}{2D}\,. \tag{8}$$

The initial condition at the beginning of the discharge pulse $t=0$ is

$$n(r,0) = 0\,. \tag{9}$$

The resulting boundary-value problem, Eqs. (7), (8), and (9), was solved numerically to give $n(r,t)$ throughout the discharge sequence. Γ_s was assumed to have a constant nonzero value during the discharge pulse and was set equal to zero during the afterglow. Figure 3 shows the resulting

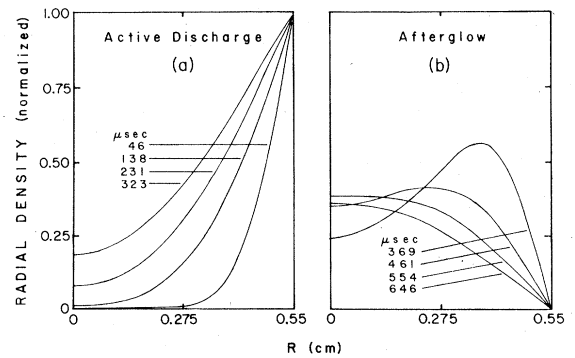

FIG. 3. Numerical solution of the boundary-value problem, Eqs. (7), (8), and (9), showing the $Cu(4s^2\,S_{1/2})$ radial density profile at various times into the discharge sequence. Data are given for a 4.1-Torr, 323-μsec discharge in a 5.5-mm radius discharge tube.

normalized radial Cu($4s^2\,S_{1/2}$) density profile $n(r,t)/(4\Gamma_s/\bar{v})$ at various times into the discharge sequence.[19] These curves were calculated using a helium pressure p_0 of 4.1 Torr, a tube radius of 5.5 mm, a discharge pulse of 323 msec, and a diffusion coefficient $Dp_0 = 430$ cm^2 sec^{-1} Torr (as measured in Sec. V). It is worth noting that the resulting time and spatial dependence of the normalized Cu($4s^2\,S_{1/2}$) density distribution is independent of the sputtering rate Γ_s. Thus the Cu($4s^2\,S_{1/2}$) density can be changed by varying the discharge current (and hence Γ_s) without effecting the time and relative spatial dependence. It can be seen from Fig. 3 that a Cu density profile, which decays close to a fundamental mode spatial distribution within a few hundred microseconds into the afterglow, can be achieved using a discharge pulse of less than 1 msec.

IV. THEORY OF DATA ANALYSIS

The afterglow decay rate of the density of the copper ground-state atoms Cu($4s^2\,S_{1/2}$) can be determined by solving the continuity equation for this species. The continuity equation involves only losses by diffusion to the walls and losses by reactions (3)–(6). Under the experimental conditions the loss of Cu($4s^2\,S_{1/2}$) by reactions (3)–(6) can be ignored.[17] In addition, only the fundamental decay mode is significant in the late afterglow since all higher modes decay more rapidly and are unimportant in the late afterglow. Therefore, the late afterglow time dependence of the Cu($4s^2\,S_{1/2}$) density $n_{\mathrm{Cu}}(t)$ is given by

$$n_{\mathrm{Cu}}(t) = n_{\mathrm{Cu}}(0)e^{-Dt/\Lambda^2},$$

where D is the diffusion coefficient of Cu($4s^2\,S_{1/2}$) in helium. Thus, the diffusion coefficient of Cu($4s^2\,S_{1/2}$) in helium can be determined by measuring the late afterglow time dependence of the relative Cu($4s^2\,S_{1/2}$) density using the absorption technique.

The decay of the light-emission intensity $I(t)$ for lines originating from the various copper-ion excited states (denoted by j, where $j=1$ for the Cu II ground state and j increases by one for successively higher Cu II energy levels) is related to the production process of these states. Since the radiative lifetimes of these Cu II states are orders of magnitude smaller than the typical afterglow decay rates, $I(t)$ is directly proportional to the production rate of the emitting state. If a particular Cu II state (denoted by m) is produced by reactions (3)–(6), either directly or by cascading, the intensity of a line originating from this level $I_m(t)$ is

$$I_m(t) \propto \sum_i n_i(t) n_{\mathrm{Cu}}(t)\left(k_{im} + \sum_{j>m} \alpha_{jm} k_{ij}\right), \qquad (10)$$

where $n_i(t)$ is the time-dependent density of a particular active helium species, k_{ij} is the reaction-rate coefficient associated with the active helium species denoted by i and the Cu II state denoted by j, and α_{jm} is the probability for the Cu II level denoted by j to decay, either directly or by cascading, to the Cu II level denoted by m [$i=1$ for He^+, $i=2$ for He_2^+, $i=3$ for $He^m(2^3S)$, and $i=4$ for $He_2^m(a^3\Sigma_u^+)$]. The late afterglow decay of $I_m(t)$ will be determined by the density $n_i(t)$ of the slowest decaying active species involved in the production process and is given by

$$I_m(t) \propto n_i(t) n_{\mathrm{Cu}}(t)\left(k_{im} + \sum_{j>m} \alpha_{jm} k_{ij}\right). \qquad (11)$$

In addition, if a state is produced by two reactions, the resulting decay rate for $I_m(t)$ will, in general, be determined in the early afterglow by the active helium species with the faster decay rate and in the late afterglow by the active helium species with the slower decay rate. Therefore, at some time into the afterglow, the decay curve for $I_m(t)$ will undergo a transition between these two regimes. This transition happens at a time into the afterglow determined by the ratio of the two production terms present in Eq. (10).

Using Eq. (11) it is possible to determine which reaction mechanism populates a given copper excited state in the late afterglow. From Eq. (11) it follows that

$$\log \frac{I_m(t)}{n_{\mathrm{Cu}}(t)} = \log n_i(t) + \text{const.} \qquad (12)$$

Therefore, a graph of Eq. (12) for various times in the late afterglow should be linear with a slope of one when the correct active helium species density $n_i(t)$ is used. Only relative values (values proportional to the absolute values) of $I_m(t)$, $n_{\mathrm{Cu}}(t)$, and $n_i(t)$ are required for this method of data analysis. Relative values for $I_m(t)$, $n_{\mathrm{Cu}}(t)$, $n_{\mathrm{He}^m}(t)$, and $n_{\mathrm{He}_2^m}(t)$ can be determined using light-emission and absorption spectroscopy. The He^+ density $n_{\mathrm{He}^+}(t)$ cannot be determined directly by optical means. However, for helium pressures above 4.5 Torr, the He^+ decay is production controlled by the reaction[20]

$$\mathrm{He}^m(2^3S) + \mathrm{He}^m(2^3S) \rightarrow \mathrm{He}^+ + \mathrm{He} + e,$$

hence, $n_{\mathrm{He}^+}(t) \propto [n_{\mathrm{He}^m}(t)]^2$. Thus a plot of Eq. (12) using $n_i = n_{\mathrm{He}^m}$ should be linear with a slope of two for those Cu II states produced by reaction (3). The He_2^+ density cannot be easily inferred using optical means and other methods must be used to identify those Cu II levels produced by reaction (4).

V. RESULTS AND DISCUSSION

Investigations were first conducted on the time dependence of the ground-state Cu($4s^2\,S_{1/2}$) number density for several pressures from 2 to 16 Torr and for discharge currents of 0.5 to 5.6 A. Figure 4 is a representative example of the resulting decay curves. In this figure, the Cu($4s^2\,S_{1/2}$) density at the center of the discharge region is plotted as a function of time into the afterglow for a helium pressure of 4.1 Torr, a discharge current of 0.6 A, and a pulse width of 320 μsec. The Cu($4s^2\,S_{1/2}$) density was determined from the fractional absorption of the 324.8-nm Cu resonance line using standard absorption techniques.[14,21]

From Fig. 4 it can be seen that a Cu($4s^2\,S_{1/2}$) density of 4×10^{10} atoms/cm^3, which is sufficient to perform the planned afterglow studies, can be achieved using a short duration pulse. In addition, the Cu($4s^2\,S_{1/2}$) density becomes exponential after about 0.5 msec into the afterglow. This indicates that the Cu($4s^2\,S_{1/2}$) density profile has decayed close to the fundamental mode within a few hundred microseconds into the afterglow as predicted by the numerical calculations (Fig. 3). It is possible to determine the diffusion coefficient for Cu($4s^2\,S_{1/2}$) in helium from Fig. 4. The results of several such decay curves at various pressures and discharge currents give a value of $Dp_0 = 430 \pm 10$ cm^2 sec^{-1} Torr. This value requires determining only the relative Cu($4s^2\,S_{1/2}$) density and not the absolute value.

The afterglow spectrum of the He-Cu discharge was scanned from 200 to 750 nm in order to determine the spectral transitions present. The spectrum consisted of Cu I, Cu II, and He I atomic

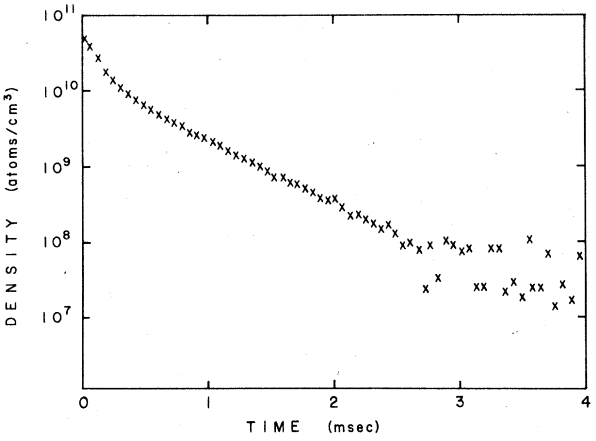

FIG. 4. Time dependence of Cu($4s^2S_{1/2}$) density during the afterglow for a pressure of 4.1 Torr, a discharge current of 0.6 A, and a discharge pulse length of 320 μsec.

TABLE I. The 35 Cu II levels monitored during the He-Cu afterglow grouped according to the time dependence of their number densities.

Group 1		Group 2	
Level	Energy (eV)	Level	Energy (eV)
$5p\,^3F_4^o$	22.70	$4p\,^3P_2^o$	15.96
$6s\,^3D_3$	24.29	$^3P_1^o$	16.15
$^3D_2$	24.31	$^3F_3^o$	16.21
$^3D_1$	24.55	$^3F_4^o$	16.25
$^1D_2$	24.56	$^3F_2^o$	16.39
$4f\,^3P_1^o$	24.57	$^3D_3^o$	16.51
$^3P_0^o$	24.58	$^3D_2^o$	16.59
$^3H_6^o$	24.58	$^1F_3^o$	16.64
$^3H_5^o$	24.58	$^3D_1^o$	16.79
$^3D_3^o$	24.59	$^1D_2^o$	16.82
$^3G_5^o$	24.61	$^1P_1^o$	16.85
$^3G_4^o$	24.62	$4s^2\,^1D_2$	18.31
		$^3P_2$	18.68
		$^3P_1$	18.71
		$^3P_0$	18.75
		$^1G_4$	19.58
		$4s4p\,^5D_4^o$	21.11
		$5s\,^3D_3$	21.12
		$^3D_2$	21.16
		$4s4p\,^5D_3^o$	21.28
		$5s\,^3D_1$	21.38
		$4s4p\,^5D_2^o$	21.41
		$5s\,^1D_2$	21.41

lines; of the Cu II spectral lines observed, 43 were of sufficient intensity to be used to monitor the decay rates of various Cu II energy levels. These lines originated from 35 Cu II levels between the energies of 15.96 and 24.62 eV listed in Table I. The notation of Moore[22] has been used to identify the levels. It was found that these levels could be divided into two groups, with levels in the same group having the same time dependence in the afterglow for all conditions studied. Group 1 consists of 12 Cu II energy levels with energies between 22.7 and 24.62 eV. Group 2 consists of 23 Cu II energy levels with energies between 15.96 and 21.41 eV. Representative decays for each group are shown in Fig. 5. The data show that the population density of the levels in group 1 had a faster decay rate than the levels in group 2. This phenomenon was observed for

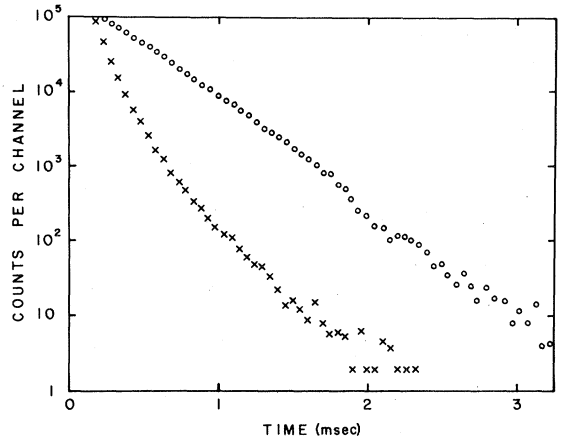

FIG. 5. Decay curves for the line-emission intensities of Cu II levels in group 1 (x) and group 2 (○) for a pressure of 11 Torr, a discharge current of 4 A, and a discharge pulse length of 700 μsec.

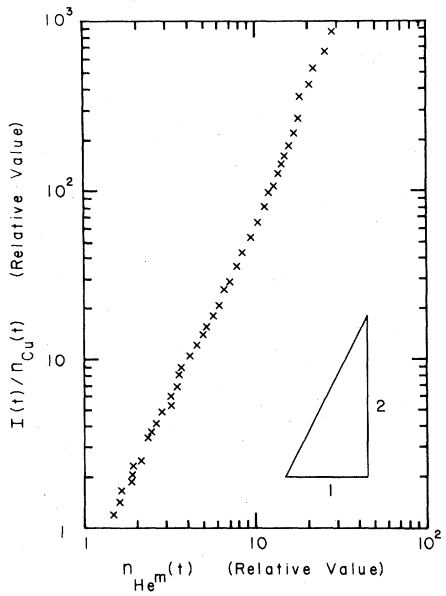

FIG. 6. Graph of relation (12) for the 491.0-nm Cu II line from the $4f^3H_6^0$ level in group 1 and for the $He^m(2^3S)$ density during the afterglow period for a pressure of 5.5 Torr, a discharge current of 0.6 A, and a discharge pulse length of 600 μsec. Each data point corresponds to the values of the relative densities and intensity at a given time into the afterglow.

all experimental conditions studied. This indicates that two separate reaction mechanisms are responsible for the production of the Cu II levels studied.

All of the levels in group 1, except the $5p\,^3F_4^0$ state, are in close resonance with He^+ as can be seen in Fig. 1. To determine if these levels are indeed produced from He^+ by reaction (3), a graph of $\log[I_m(t)/n_{Cu}(t)]$ versus $\log n_{He^m}(t)$ is plotted as discussed in the previous section. Figure 6 shows such a plot for the 491.0-nm transition originating from the $4f^2H_6^0$ Cu II level for a helium pressure of 5.5 Torr and a discharge current of 0.6 A. The dependence is linear for the later part of the afterglow (lower particle densities) with a slope of two. This relationship was found to hold from 5 to 16 Torr for currents of 0.6 to 5.6 A. Thus it can be concluded that the 11 upper Cu II levels in group 1 are populated by He^+ through reaction (3). The $5p\,^3F_4^0$ Cu II level is probably populated by radiative cascading from these upper states.

The Cu II levels in group 2 have energies ranging from 15.96 to 21.41 eV and are energetically accessible for energy transfer from He_2^+, $He^m(2^3S)$, and $He_2^m(a^3\Sigma_u^+)$. However, several of the group 2 levels have energies above 21 eV. It is not energetically possible for these levels to be produced by either helium metastable species via reactions (5) or (6). However, they are accessible from He_2^+. Thus it can be concluded that the Cu II levels in group 2 with energies above 21 eV are produced from He_2^+ by reaction (4). This agrees with previous results on the energy-transfer mechanisms in He-Cs afterglows.[12]

The levels in group 2 with energies below 20 eV are accessible for energy transfer from $He^m(2^3S)$ and $He_2^m(a^3\Sigma_u^+)$. However, when Eq. (12) was graphed for these levels using the $He^m(2^3S)$ density for n_t, the resulting slope was unequal to one and varied with varying experimental conditions. In addition, since the $He^m(2^3S)$ density decay rate is slower than the He_2^+ density decay rate for the pressure range studied,[20] the late afterglow decay rate of these levels should be slower than the decay rate for the group 2 levels above 21 eV if reaction (5) is of importance. However, this was not the case. Therefore, none of the Cu II levels in group 2 are predominantly produced by $He^m(2^3S)$ through reaction (5).

In this experiment, the decay of the $He_2^m(a^3\Sigma_u^+)$ density could not be measured by absorption. The absorber number density of $He_2^m(a^3\Sigma_u^+, \nu=0)$ was too small and the scattered background light was too intense to allow for reliable measurements. However, since the $He_2^m(a^3\Sigma_u^+)$ density decay rate is slower than the He_2^+ density decay rate,[20] the late afterglow decay of the group 2 levels below 18 eV should be slower than the decay rate of the group 2 levels above 21 eV if reaction (6) is important. This did not occur. Hence, none of the Cu II levels in group 2 are predominantly produced by $He_2^m(a^3\Sigma_u^+)$ via reaction (6).

From the above results, it can be concluded

that all the Cu II levels in group 2 are predominantly produced by He_2^+ via reaction (4). Further support for this conclusion can be found by investigating the shape of the decay curves for the Cu II levels in group 2. As can be seen from Fig. 5, these curves deviate from a simple exponential decay in the very late afterglow. This effect is similar to the deviation observed in the decay curves of ions studied in afterglows using mass spectroscopy. In the case of ions this effect is due to the transition from ambipolar to free-diffusion.[23] This similarity indicates that the Cu II levels in group 2 are produced by ions undergoing a transition from ambipolar to free-diffusion. Since these levels decay differently than the group 1 levels produced by He^+, they must be produced by He_2^+.

Further information about the nature of reaction (4) can be obtained by studying the dependence on the energy defect of the reaction-rate coefficients k_{2j} for producing specific Cu II excited states from He_2^+. Since the levels in group 2 are produced, either directly or by cascading, by the two reactions (3) and (4), the decay curves for the intensity of spectral lines from the group 2 states will undergo the transition in decay rates discussed in the previous section. This transition in decay rates was observed for the spectral lines from the Cu II levels in group 2, with the early afterglow decay of these lines having the same time dependence as the decay of the lines from the Cu II levels in group 1. The spectral lines from the group 2 levels between 18 and 20 eV underwent this transition at a much earlier time into the afterglow than did the spectral lines from other group 2 states. This occurred for all experimental conditions studied.

As discussed in Sec. IV, the time into the afterglow at which this transition occurs for spectral lines from a particular Cu II level (denoted by m) is determined by the ratio

$$n_1(t)\left(k_{1m}+\sum_{j>m}\alpha_{jm}k_{1j}\right)\Big/\, n_2(t)\left(k_{2m}+\sum_{j>m}\alpha_{jm}k_{2j}\right).$$

Therefore, if it is assumed that the term $(k_{1m}+\sum_{j>m}\alpha_{jm}k_{1j})$ is approximately the same for all Cu II states in group 2, the term $(k_{2m}+\sum_{j>m}\alpha_{jm}k_{2j})$ is larger for the group 2 levels between 18 and 20 eV than for the other group 2 levels. Since the difference in time into the afterglow at which the transition in decay rates occurred was much larger than could be accounted for by differences in the term $\sum_{j>m}\alpha_{jm}k_{2j}$, the reaction-rate coefficients k_{2j} are larger for the group 2 levels between 18 and 20 eV than for the other group 2 levels. In addition, the intensities for spectral lines from the Cu II states in group 2 above 20 eV were much weaker than the intensities for lines from group 2 levels below 20 eV. This also indicates that the reaction-rate coefficients k_{2j} are larger for the group 2 states immediately below 20 eV than for the group 2 states above 20 eV. Therefore, the reaction-rate coefficients for reaction (4) are larger for production of Cu II levels between 18 and 20 eV, involving energy defects of 2.6 to 4 eV, then for the other Cu II levels produced by reaction (4) involving smaller or larger energy defects.

This observed energy-defect dependence of the reaction-rate coefficient for reaction (4) can be explained by assuming that this reaction proceeds as

$$He_2^+ + Cu \rightarrow (Cu^+)^* + (He_2)_r \longrightarrow 2He, \qquad (13)$$

where $(He_2)_r$ is the molecular helium repulsive ground state.[12,24,25] The excess energy is then carried off as kinetic energy by the two neutral helium atoms. From the potential energy curves for He_2^+ and $(He_2)_r$, and assuming state transitions at constant internuclear separation, the available energy for the excitation of Cu II levels by He_2^+ via process (13) is 18.7 to 20.4 eV.[12] Thus the reaction-rate coefficient for reaction (13) should be largest for the production of Cu II states between 18.7 and 20.4 eV. This agrees with the observed energy-defect dependence of the production rate of the Cu II energy levels in group 2.

It was not possible to determine the reaction rate coefficients for reactions (3)–(6) due to the nature of the copper sputtering process. When copper is sputtered from a surface it is ejected as single atoms, but forms clusters of two or more atoms just above the sputtering surface.[26-28] These clusters can act as efficient deexcitation centers for the active helium species and significantly alter their decay rates. This effect was observed for the $He^m(2^3S)$ decays and became more pronounced at higher sputtering rates (higher discharge currents). The decay rate of $He^m(2^3S)$ was increased by up to 20% by this effect. Thus, any attempt to measure the reaction-rate coefficients for reaction (3)–(6) would lead to erroneously large values.

VI. CONCLUSIONS

Measurements were performed on the stationary afterglow of a He-Cu discharge utilizing copper sputtered into the vapor phase. The radial profile of the sputtered copper atoms $Cu(4s^2\,S_{1/2})$ was modeled during the discharge sequence in order to determine the time scale involved in establishing a $Cu(4s^2\,S_{1/2})$ density during the active dis-

charge which would decay close to the fundamental diffusion mode spatial distribution within a few hundred microseconds into the afterglow. The decay of the Cu($4s^2\,S_{1/2}$) density was measured by absorption. It became exponential within 0.5 msec into the afterglow after achieving densities on the order of 4×10^{10} atoms/cm^3 at the end of the active discharge pulse. From these decays, the diffusion coefficient of Cu($4s^2\,S_{1/2}$) in helium was determined to be $Dp_0 = 430 \pm 10$ cm^2 sec^{-1} Torr.

The decays of the emission intensities for 43 lines originating on the 35 Cu II levels listed in Table I were monitored to determine the energy-transfer mechanisms between the active helium species [He^+, He_2^+, $He^m(2^3S)$, and $He_2^m(a^2\Sigma_u^+)$] and Cu($4s^2\,S_{1/2}$). These levels formed two groups when classified according to their decay rates. The 12 levels in group 1 with energies between 22.7 and 24.62 eV are populated by charge transfer from He^+. The 23 levels in group 2 with energies between 15.96 and 21.41 eV are populated by charge transfer from He_2^+. There was no evidence for the population of Cu II levels by the Penning ionization of Cu($4s^2\,S_{1/2}$) by $He^m(2^3S)$ or $He_2^m(a^3\Sigma_u^+)$. The dependence on the energy defect of the reaction-rate coefficients for energy transfer between He_2^+ and Cu($4s^2\,S_{1/2}$) indicated that reaction (4) occurs through a dissociative charge-transfer mechanism [reaction (13)].

It was not possible to determine the reaction-rate coefficients for these charge-transfer processes due to the formation of copper clusters. These clusters can significantly alter the decay rates of the active helium species, making measurements of the reaction-rate coefficients impossible in this experimental arrangement.

ACKNOWLEDGMENT

This work was supported by the National Science Foundation under Grant No. ENG 78-25933.

[1]W. T. Silfast, Appl. Phys. Lett. 13, 169 (1968).
[2]R. C. Jensen, G. J. Collins, and W. R. Bennett, Jr., Phys. Rev. Lett. 23, 363 (1969).
[3]W. T. Silfast and M. B. Klein, Appl. Phys. Lett. 17, 400 (1970).
[4]L. Csillag, M. Jånossy, K. Rôzsa, and T. Salamon, Phys. Lett. 50A, 13 (1974).
[5]J. R. McNeil, G. J. Collins, K. B. Persson, and D. L. Franzen, Appl. Phys. Lett. 27, 595 (1975).
[6]J. R. McNeil, W. L. Johnson, G. J. Collins, and K. B. Persson, Appl. Phys. Lett. 29, 172 (1976).
[7]R. D. Reid, J. R. McNeil, G. J. Collins, Appl. Phys. Lett. 29, 666 (1976).
[8]A. R. Turner-Smith, J. M. Green, and C. E. Webb, J. Phys. B 6, 114 (1973).
[9]G. J. Collins, J. Appl. Phys. 44, 4633 (1973).
[10]J. M. Green and C. E. Webb, J. Phys. B 7, 1698 (1974).
[11]E. Graham IV, M. A. Biondi, and R. Johnsen, Phys. Rev. A 13, 965 (1976).
[12]C. P. de Vries and H. J. Oskam, Phys. Rev. A 19, 2095 (1979).
[13]D. Rosenberg and G. K. Wehner, J. Appl. Phys. 33, 1842 (1962).
[14]A. Mitchell and M. Zemansky, *Resonance Radiation and Excited Atoms* (Cambridge University Press, Cambridge, 1961), Chap. 3.
[15]R. V. Stuart and G. K. Wehner, J. Appl. Phys. 35, 1819 (1964).
[16]If a hard-sphere model is assumed for the elastic collision between copper and helium atoms, the sputtered copper atoms lose an average of 11% of their energy in each collision. Thus they reach thermal energy $kT = 0.025$ eV after an average of 32 collisions. Since the copper atoms are much more massive than the helium atoms, they undergo only small average deflections during each collision. Therefore, after 32 collisions, the copper atoms are still traveling in approximately the same direction in which they were sputtered, having traveled a distance of approximately $32\lambda_0$, where λ_0 is the mean-free path of copper in helium. λ_0 can be approximated by the mean-free path of helium in helium of 3×10^{-3} cm at 5 Torr. Finally, if the copper atoms are assumed to be sputtered isotropically, the average distance from the sputtering surface traveled by the copper atoms before they thermalize is $\frac{1}{2}(32\lambda_0) = 0.48$ mm.

[17]If the copper atoms are lost by reactions (3)–(6), the volume-loss frequency due to each reaction is $k_i n_i$, where k_i is the reaction-rate coefficient for the reaction and n_i is the density of the active helium species involved. If we assume $k_i < 10^{-9}$ cm^3 sec^{-1} and $n_i < 10^{10}$ cm^{-3}, both of which are reasonable assumptions for the afterglow conditions, the volume-loss frequency is less than 10 sec^{-1}. The diffusion-loss frequency for copper atoms D/Λ^2 is $8130/p_0$. Therefore, the contribution to the total loss frequency due to reactions (3)–(6) can be ignored under the experimental conditions. This is verified experimentally by varying n_i by changing the discharge parameters (pressure and discharge current) and looking for any corresponding changes in the decay rate of the copper atoms. No such effects were observed. Finally, it should be noted that the above analysis also applies to the various active helium species. Since $n_{Cu} < 10^{10}$ cm^{-3} during the major part of the afterglow, $k_i n_{Cu} < 10$ sec^{-1} for the processes (3)–(6). Therefore, the contribution from these processes to the loss frequency of the active helium species can also be ignored in the late afterglow.

[18]G. N. Hays, C. J. Tracy, and H. J. Oskam, J. Chem. Phys. 60, 2027 (1974).
[19]The normalization factor $4\Gamma_s/\bar{v}$ used in graphing Fig. 3 is determined by considering the value of $n(r,t)$ in an active discharge as $t\to\infty$. As $t\to\infty$, the processes of production of copper atoms by sputtering and loss of copper atoms by diffusion to the walls come to equilibrium. Therefore, as $t\to\infty$, $\vec{\Gamma}(r,t) = -D[\partial n(r,t)/\partial r] \times \hat{r} \to 0$. Thus, $n(r,t) \to$ const as $t\to\infty$. From Eq. (8), $n(r,t) \to 4\Gamma_s/\bar{v}$ as $\vec{\Gamma}(r,t) \to 0$. Hence, $n(r,t) \to 4\Gamma_s/\bar{v}$ as

$t \to \infty$. This result also follows from the analytical solution to the boundary-value problem. This value was used as the normalization factor in Fig. 3.

[20]R. Deloche, P. Monchicourt, M. Cheret, and F. Lambert, Phys. Rev. A 13, 1140 (1976).

[21]The absorption was performed on a cylindrical region in the discharge volume coaxial with the discharge tube axis and 3 mm in radius. The $Cu(4s^2S_{1/2})$ density at the center of the discharge tube was determined from the resulting fractional absorption after adjusting for the fundamental mode spatial distribution of the $Cu(4s^2S_{1/2})$ density in the absorption region. An oscillator strength of $f = 0.43$ was used in the calculations [Graydon D. Bell and Eldred F. Tubbs, Astrophys. J. 159, 1093 (1970)]. Since the 324.8-nm CuI line is composed of 12 hyperfine transitions forming two resolvable components [N. L. Moise, Astrophys. J. 144, 774 (1966)], this effect was also taken into account.

[22]C. E. Moore, *Atomic Energy Levels* (U. S. Government Printing Office, Washington, D. C., 1952), Vol. II.

[23]R. A. Gerber and J. B. Gerardo, Phys. Rev. A 7, 781 (1973).

[24]J. J. Leventhal, J. D. Earl, and H. H. Harris, Phys. Rev. Lett. 35, 719 (1975).

[25]D. W. Ernie and H. J. Oskam, Phys. Rev. A 21, 95 (1980). A dissociative excitation-transfer process analogous to process (12) is discussed in this paper.

[26]James R. Woodyard and C. Burleigh Cooper, J. Appl. Phys. 35, 1107 (1964).

[27]J. W. Coburn, E. W. Eckstein, and Eric Kay, J. Vac. Sci. Technol. 12, 151 (1975).

[28]W. Gerhard and H. Oechsner, Z. Phys. B 22, 41 (1975).